

## Field-Free Nucleation of Antivortices and Giant Vortices in Nonsuperconducting Materials

Morten Amundsen,<sup>\*</sup> Jabir Ali Ouassou, and Jacob Linder

Center for Quantum Spintronics, Department of Physics, Norwegian University of Science and Technology, NO-7491 Trondheim, Norway

 (Received 12 December 2017; revised manuscript received 24 February 2018; published 14 May 2018)

Giant vortices with higher phase winding than  $2\pi$  are usually energetically unfavorable, but geometric symmetry constraints on a superconductor in a magnetic field are known to stabilize such objects. Here, we show via microscopic calculations that giant vortices can appear in intrinsically nonsuperconducting materials, even without any applied magnetic field. The enabling mechanism is the proximity effect to a host superconductor where a current flows, and we also demonstrate that antivortices can appear in this setup. Our results open the possibility to study electrically controllable topological defects in unusual environments, which do not have to be exposed to magnetic fields or intrinsically superconducting, but instead display other types of order.

DOI: [10.1103/PhysRevLett.120.207001](https://doi.org/10.1103/PhysRevLett.120.207001)

*Introduction.*—It is well known that applying a magnetic field to a type-II superconductor can lead to the formation of Abrikosov vortices [1]. A gradient in the phase  $\varphi$  of the superconducting order parameter  $\Delta = |\Delta|e^{i\varphi}$  causes a circulating supercurrent around such vortices, whereas  $|\Delta| \rightarrow 0$  at their centers. Vortex excitations in superconductors [2,3] remains a vibrant research topic, not least because it lies at the intersection of two major research fields: superconductivity and topology in physics.

It was recently pointed out in Ref. [4] that it is also possible to generate Josephson vortices without applying magnetic fields. Such vortices are also characterized by a quantized phase winding and a suppressed order parameter at their core [5]. Motivated by this, we have performed microscopic calculations using the quasiclassical theory of superconductivity [6] on a normal metal enveloped by a current-biased superconducting wire (Fig. 1). The idea behind the device is simple: an external current source forces a supercurrent through the wire, and this circulation whirls the condensate in a proximitized normal metal as well. Our objective has been to determine what type of electrically controllable vortex physics then emerges. We demonstrate here that both giant vortices and antivortices appear in the nonsuperconducting region even in the absence of any applied magnetic field. This provides an alternative method of creating complex vortex patterns by applying electric currents. Since these patterns are generated in a proximitized nonsuperconductor, this opens up the intriguing prospect of studying unusual topological vortex excitations in materials with other types of quantum order, which do not have to be compatible with bulk superconductivity. One example is a magnetic metal, where the generation of odd-frequency triplet superconducting order could reverse the chirality of some vortices, similarly

to the paramagnetic Meissner effect [7,8]. More fundamentally, it raises the intriguing question: what characterizes a vortex in an odd-frequency order parameter?

*Geometric effect and winding number.*—Since a circulating supercurrent requires a finite phase-gradient  $\nabla\varphi$ , and the analyticity of the superconducting wave function implies integral winding numbers  $n = \Delta\varphi/2\pi$  around any point, the system is topologically coerced into nucleating vortices in the normal metal region of Fig. 1. Assuming a thin-film structure, the total charge current associated with this circulation is small, and the magnetic field generated by the circulation can safely be neglected. Note that in contrast to the setup proposed in Ref. [4], our normal metal is surrounded by a continuous superconducting wire on all sides, instead of having two separate wires on the top and bottom, which we will show fundamentally alters the vortex physics in the system. Another important difference is that we model the superconducting wire using an exact solution

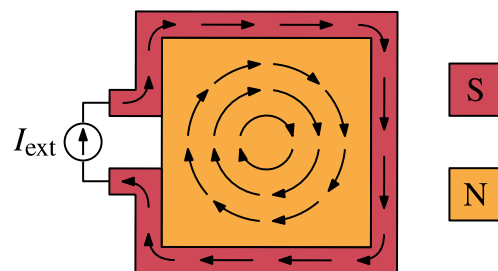


FIG. 1. Conceptual sketch of the physical system. An external current source is used to inject a current into a superconductor (red). The circulating current also affects a proximitized normal metal (yellow), causing an electrically controlled vortex to emerge there.

of the Usadel equation in the current-biased superconductor and tunneling boundary conditions. As we will demonstrate, this is necessary to correctly describe qualitative changes that the phase winding induces in, e.g., the density of states (DOS).

When the current in the superconducting wire makes a total winding number  $N > 1$ , there are multiple ways to satisfy the boundary conditions. Among other possibilities, we can get (i)  $N$  vortices with a winding 1 each, (ii)  $N + M$  vortices with a winding +1 and  $M$  antivortices with winding  $-1$ , or (iii) just one giant vortex with a winding  $N$ . The kinetic energy of an  $n$ -winding vortex scales with  $n^2$ , so the most energetically favorable is configuration (i). Hence, giant vortices and antivortices are seldom seen. However, since the superconducting order parameter respects the symmetries of the underlying geometry, vortices only nucleate along the symmetry axes of the system. For highly symmetric geometries, these additional constraints may force the appearance of giant vortices or antivortices. The resulting interplay between topological defects, geometric symmetries, and energy minimization was previously studied in Refs. [9–12] using the phenomenological Ginzburg-Landau formalism for type-II superconductors in a magnetic field. Here, we show that this effect also arises in proximitized normal metals without magnetic fields. This generalization is particularly important as it opens the possibility to study novel vortex physics in materials featuring completely different order than superconductors, e.g., ferromagnets or topological insulators.

*2D diffusive metal with phase-winding.*—As shown in Fig. 1, we consider a normal metal with a superconducting loop grown on top. We describe the properties of the metal in terms of quasiclassical propagators  $\hat{g}$  in Nambu and spin space,

$$\hat{g}(\mathbf{r}, \epsilon) = \begin{pmatrix} g(\mathbf{r}, +\epsilon)\sigma_0 & f(\mathbf{r}, +\epsilon)i\sigma_2 \\ -f^*(\mathbf{r}, -\epsilon)i\sigma_2 & -g^*(\mathbf{r}, -\epsilon)\sigma_0 \end{pmatrix}, \quad (1)$$

where the normal part  $g$  and anomalous part  $f$  are complex scalar functions, subject to the normalization constraint  $\hat{g}^2 = 1$ . Here,  $\sigma_0$  is the  $2 \times 2$  identity matrix, and  $\sigma_2$  is the second Pauli matrix. We assume that all length scales in the problem are large compared to the Fermi wavelength and mean free path; i.e., we take the quasiclassical diffusive limit. The propagators  $\hat{g}$  are then governed by the Usadel equation [6,13,14],

$$D\nabla(\hat{g}\nabla\hat{g}) + i[\epsilon\hat{\tau}_3, \hat{g}] = 0, \quad (2)$$

where  $D$  is the diffusion constant,  $\epsilon$  the quasiparticle energy, and  $\hat{\tau}_3 = \text{diag}(+\sigma_0, -\sigma_0)$ . Furthermore, we assume that the normal region is connected to the superconducting wire by a low-transparency interface. We may then use the Kupriyanov-Lukichev boundary condition  $\zeta\mathbf{e}_\perp \cdot \nabla\hat{g}_n = [\hat{g}_n, \hat{g}_s]/\xi$  [15], where  $\zeta$  parametrizes interface resistance,

$\mathbf{e}_\perp$  is the outwards-pointing interface normal vector,  $\hat{g}_n$  and  $\hat{g}_s$  are propagators on the normal and superconducting sides, and  $\xi$  the superconducting coherence length. The propagators  $\hat{g}_s$  in the current-biased superconductors were evaluated analytically. The applied current also creates a magnetic field which penetrates the proximitized material. Its strength depends on the total applied current, which in turn depends on the pair density and dimensions of the superconductor. However, since the field is perpendicular to and roughly constant within the current loop, its only effect is to slightly perturb the applied current for which a given vortex pattern appears. We have neglected the quantitative correction from the magnetic field herein.

In practice, the differential equations above are Riccati-parametrized for stability [16], and then solved numerically using a finite-element method on a two-dimensional mesh. This lets us handle arbitrary sample geometries, such as the regular polygons considered herein. For more information about the numerical solution procedure itself, see Ref. [17].

*Superconducting wire with a uniform current.*—As shown in Sec. II of the Supplemental Material [18], the propagator  $\hat{g}$  in a current-biased bulk superconductor can be written [23,24]

$$\hat{g} = \frac{1}{\sqrt{\epsilon^2 - \Theta^2}} \begin{pmatrix} +\epsilon\sigma_0 & \Theta e^{+i\varphi}i\sigma_2 \\ \Theta e^{-i\varphi}i\sigma_2 & -\epsilon\sigma_0 \end{pmatrix}, \quad (3)$$

where  $\Theta(\epsilon)$  parametrizes the strength of the superconductivity, and  $\varphi$  is the superconducting phase. The phase varies linearly with the distance  $\ell$  along the wire. Defining  $\varphi(0) \equiv 0$ , and parametrizing the variation using a winding rate  $u \equiv \xi|\nabla\varphi|$ , we therefore get  $\varphi(\ell) = u\ell/\xi$ . The function  $\Theta(\epsilon)$  is determined by

$$\Theta = \frac{|\Delta|}{1 + u^2/2\sqrt{\Theta^2 - \epsilon^2}}, \quad (4)$$

$$|\Delta| = \frac{1}{\text{acosh}\omega_c} \int_0^{\omega_c} d\epsilon \text{Re} \left( \frac{\Theta}{\sqrt{\epsilon^2 - \Theta^2}} \right) \tanh \left( \frac{\pi\epsilon}{2e^\gamma T} \right). \quad (5)$$

These equations have been written in a form where  $\Theta$ ,  $\Delta$ ,  $\epsilon$ ,  $\omega_c$  are all normalized to the zero-current gap  $\Delta_0$ , while the temperature  $T$  is normalized to the critical temperature  $T_c$ . Here,  $\omega_c$  refers to the Debye cutoff, and  $\gamma$  is the Euler-Mascheroni constant. The first of these equations is a fixpoint iteration equation. This is easily solved by guessing  $\Theta(\epsilon) = 1$  and  $|\Delta| = 1$ , and applying Newton's method to the equation for a discretized set of energies from the Debye cutoff  $\epsilon = \omega_c$  to zero energy  $\epsilon = 0$ . The second is a self-consistency equation for the gap  $\Delta$ , which is evaluated by numerical integration of the results for  $\Theta(\epsilon)$ . We then alternate between solving the fixpoint equation and self-consistency equation until satisfactory convergence. The solutions to the equations above are visualized in Fig. 2.

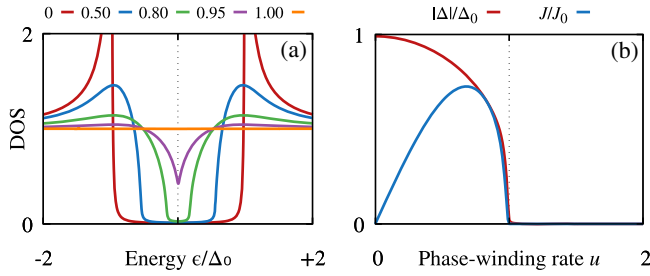


FIG. 2. Visualization of a bulk superconductor with a uniform current at zero temperature. (a) DOS for varying winding rates  $u$ , as shown in the legends above. Note how the coherence peaks are smoothed out for  $u > 0$  and the gap closes as  $u \rightarrow 1$ , illustrating a qualitatively different behavior for  $u > 0$ . (b) Gap  $\Delta$  and current density  $J$  as functions of  $u$ , where the unit  $J_0 = eDN_0\Delta_0/4\xi$ . As long as  $u < 1/2$ , we see that  $\Delta \approx \Delta_0$  and  $J \sim u$ , and a non-self-consistent solution is reasonably accurate. However, the current becomes nonmonotonic for  $u > 2/3$ , so this regime is inaccessible in our proposed setup.

When approaching the setup in Fig. 1 numerically, we assumed that the superconducting wire suffers a negligible inverse proximity effect from the normal metal. In this case, we can use the analytical equation above for the superconducting wire, and reduce the superconductor to effective boundary conditions for the normal metal. Furthermore, we numerically only considered phase-winding rates  $u \leq 0.5$ , in which case Eq. (5) can be replaced by the approximation  $|\Delta| \approx 1$ . Note that since the phase-winding rate  $u$  cannot be arbitrarily large, we need a system much larger than the coherence length to obtain high winding numbers using a current bias.

*Quantifying vortices.*—We can study the proximity-induced superconductivity in a normal metal via the pair correlation

$$\Psi(\mathbf{r}) \sim \int_0^{\omega_c} d\epsilon [f(\mathbf{r}, +\epsilon) - f(\mathbf{r}, -\epsilon)] \tanh(\epsilon/2T), \quad (6)$$

which behaves like a complex order parameter. This pair correlation can be decomposed as  $\Psi \equiv |\Psi| \exp(i\varphi)$ , and the phase  $\varphi$  can then be extracted using  $\varphi = \arctan(\text{Im}\Psi/\text{Re}\Psi)$ .

As discussed in the introduction, the circulating current in the enclosing superconductor creates a phase-winding  $\nabla\varphi$  along the interface. However, the phase  $\varphi$  is uniquely defined modulo  $2\pi$ , which means that it is only possible for the phase to vary continuously around the edges of the normal metal if it increases by  $\Phi_I = 2\pi N$  after having traversed the entire circumference. In other words, we must have a total vorticity

$$N = \frac{\Phi_I}{2\pi} \equiv \frac{1}{2\pi} \oint_{\partial\Omega} (\nabla\varphi) \cdot d\ell, \quad (7)$$

where  $\partial\Omega$  is the boundary of the normal metal. When we have a finite vorticity  $N$ , the currents inside the normal

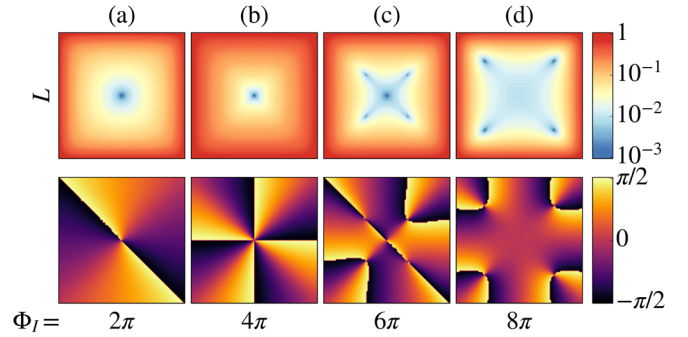


FIG. 3. Vortex nucleation patterns for various applied current windings  $\Phi_I$ , for a quadratic normal metal with side lengths  $L = 12\xi$ . The top row shows the magnitude  $|\Psi|$  of the pair correlation, where the minima indicate the vortices. The bottom row shows the phase  $\varphi$  of the pair correlation, from which the winding of individual vortices can be determined. The total windings  $\Phi_I$  are listed below.

metal will form closed loops, leading to the appearance of vortices. More precisely, the total vorticity  $N$  will be equal to the sum of the winding numbers  $n$  of all the induced vortices. The vortices manifest as nodes in the pair correlation  $\Psi$ .

*Numerical results.*—In the upper row of Fig. 3, the vortex pattern for increasing applied current winding  $\Phi_I$  is shown. The winding of the individual vortices may be determined graphically from the phase of the pair correlation function  $\varphi$ , which is plotted in the bottom row of Fig. 3. By using Eq. (7) with the replacements  $N \rightarrow n$  and  $\partial\Omega \rightarrow \mathcal{C}$ , where  $\mathcal{C}$  is any contour encircling a single vortex, one sees that  $n \neq 0$  only if the integration path crosses discontinuities. Furthermore, each discontinuity contributes a value to the integral equal to the size of the jump. For  $\Phi_I = 2\pi$ , shown in Fig. 3(a), there is a single vortex in the center of the normal metal, and any closed contour around this point must traverse two jumps  $\Delta\varphi = \pi$ , thus showing that the vortex has a winding  $n = +1$ . We note that the precise locations of these discontinuities depend on the reference point for the phase of the superconductors, and are hence not physically significant. The number of times a closed loop crosses a discontinuity, however, is. In Fig. 3(b), where  $\Phi_I = 4\pi$ , there is still only a single vortex in the system, but now the plot of  $\varphi$  shows four discontinuities, from which it is inferred that this is a giant vortex with  $n = +2$ .

For  $\Phi_I = 6\pi$ , shown in Fig. 3(c), five vortices are found. As the sum of the individual topological numbers should add up to  $N = +3$ , in accordance with Eq. (7), one of these vortices must be an antivortex. The phase plot shows that this is indeed the case: the central vortex winds in the opposite direction of other vortices. Hence, this configuration consists of one central  $n = -1$  antivortex with four surrounding  $n = +1$  vortices. For  $\Phi_I = 8\pi$ , there are four regular  $n = +1$  vortices along the diagonals, as shown in Fig. 3(d). Since these vortex patterns arise from symmetry constraints, they are naturally sensitive to asymmetries in

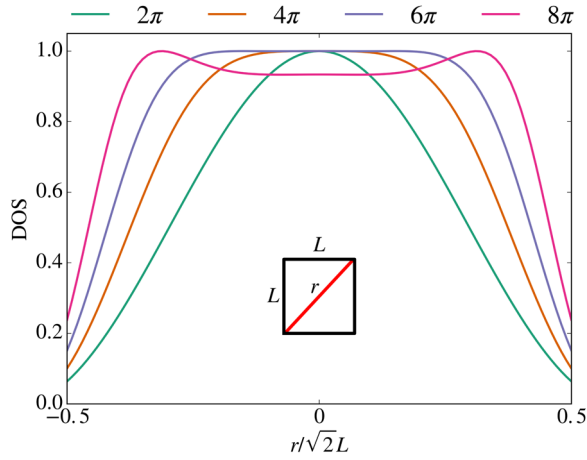


FIG. 4. DOS along the diagonal of the normal metal for various applied current windings  $\Phi_J$ . Superconductivity is suppressed in the vortex cores, and the normal-state DOS = 1 is recovered.

the geometry. The giant vortex in Fig. 3(b) splits into two  $n = +1$  vortices as the geometry becomes rectangular. However, the vortices continue to overlap strongly for sufficiently small deviations, as shown in Sec. III of the Supplemental Material [18]. This means that the giant vortex could in practice be stabilized against deviations from perfect symmetry by creating a pinning potential at this location [25]. Since the vortex positions are also influenced by the applied currents, another option is to fine-tune the currents to experimentally realize the giant vortex. The pattern in Fig. 3(c) is, on the other hand, stable against small deviations in aspect ratio. The reason is that when the geometry becomes increasingly rectangular, it eventually becomes energetically favorable to satisfy  $N = +3$  as three  $n = +1$  vortices along the longest axis. The transition to such a pattern can only occur in a way which respects the symmetries of the rectangle, and hence the central antivortex turns into a vortex, and additional antivortices must appear so that the off-center vortices can annihilate symmetrically [26].

The vortices also create a spatial modulation of the DOS: at the vortex cores, superconductivity vanishes, and the minigap disappears. This means that the vortices we predict can be directly inferred via local STM measurements. In Fig. 4, the DOS for  $\epsilon = 0$  is plotted along the diagonal of the normal metal (i.e., between two opposite corners). This confirms that the normal-state result DOS = 1 is recovered at the vortex cores. For the  $n = +2$  vortex produced by  $\Phi_J = 4\pi$ , the minigap is suppressed in a larger region around the vortex than for  $\Phi_J = 2\pi$ . For  $\Phi_J = 6\pi$ , the normal region is larger still, but this is likely due to the close proximity of three vortices. For  $\Phi_J = 8\pi$ , the vortices are sufficiently far apart for a dip in the DOS to appear in between, providing an observable signature.

The above can be understood by analyzing the pair correlation. In Sec. I of the Supplemental Material [18], it is shown that for small distances  $r$  from the vortex center,

$\Psi \sim (r/2\xi_0)^n/n!$ , where  $\xi_0$  is the Ginzburg-Landau coherence length. For  $r < 2\xi_0(n!)^{1/n} \approx 2[1 + (n-1)/e]\xi_0$ , these correlations recover more slowly with increasing winding  $n$ , and hence the minigap is increasingly suppressed. The fact that the vortex size increases linearly with  $n$  also in the diffusive limit can be motivated from Fig. 2. There, we see that superconductivity vanishes entirely as the phase-winding rate  $u \equiv \xi|\nabla\varphi| \rightarrow 1$ . Assuming that this remains approximately valid in nonbulk materials, and using that  $|\nabla\varphi| = |n|/r$  around an  $n$ -winding vortex, we find that superconductivity vanishes for  $r < n\xi$ . In other words, we find that the core size of a giant vortex scales linearly with its winding number  $n$ , providing an observational signature of giant vortices that can be seen via STM measurements.

The vortex patterns of Fig. 3 may be deduced from energy considerations. In general, the kinetic energy of a vortex with a winding number  $n$  scales as  $n^2$ . This is because kinetic energy  $E_k \sim v^2$ , where  $v \sim \nabla\varphi \sim n$  is the velocity of the superconducting condensate. In Sec. I of the Supplemental Material [18], we solve the linearized Ginzburg-Landau equation near a vortex with winding number  $n$ , and use this to confirm that the kinetic energy is indeed proportional to  $n^2$ . Similar  $n^2$  dependencies have previously been noted for magnetic vortices in type-II superconductors [27], and these properties are shared by vortices in proximitized nonsuperconductors [5,28].

The above provides a simple prescription for predicting the vortex nucleation pattern. When a total vorticity  $N$  is introduced to the system, it splits into vortices with individual windings  $n_i$  in a way that satisfies  $N = \sum_i n_i$ . Among all patterns permitted by the symmetries of the geometry, the energetically favored is the one that minimizes  $E = \sum_i n_i^2$ . Note that  $n_i$  can be either positive or negative, allowing for antivortex nucleation.

In the geometry considered so far, off-center vortices can only appear in a square formation without breaking the symmetry of the system, as is seen in Fig. 3. This symmetry constraint explains why it is possible to produce a vortex with winding  $n = +2$ . A higher winding is, however, not possible because it will always be energetically favorable to introduce four new vortices away from the center, and, potentially, an antivortex in the center. Similar results were found for a mesoscopic superconductor in an applied magnetic field [10–12]. The present analysis differs in that the vortex patterns are generated in an intrinsically non-superconducting material solely by an applying an electric current. A regular polygon with a higher symmetry (larger number of sides), will by the same reasoning as above allow for a higher winding at the center, as any alternative will require a larger number of  $n = +1$  vortices to be distributed in a symmetrical fashion. Figure 5 shows the pair correlation function for a hexagonal normal metal surrounded by a superconductor with an applied current equivalent to  $\Phi_J = 6\pi$ . Here, we find a single vortex of

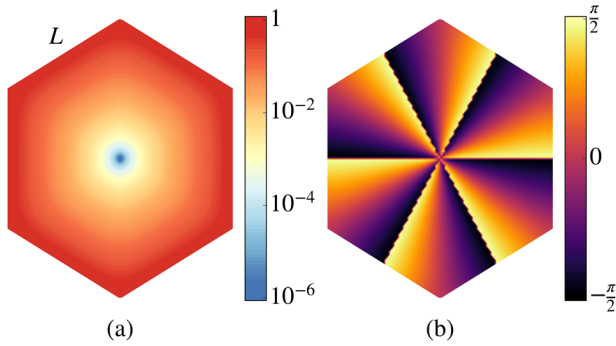


FIG. 5. Hexagonal geometry with side lengths  $L = 6\xi$ , and an applied current winding  $\Phi_I = 6\pi$ . (a) The pair correlation  $\Psi$ , showing a single vortex at the center. (b) The phase  $\varphi$  of the pair correlation, demonstrating that it is a giant vortex with winding number  $n = +3$ .

winding  $n = +3$ . Generally, a regular polygon with  $m$  sides allows for a giant vortex with winding up to  $n = \lfloor m/2 \rfloor$ .

*Conclusion.*—We have used microscopic calculations to show that one can induce giant vortices and antivortices in nonsuperconducting materials in the absence of magnetic fields. We also analyzed the vortex nucleation pattern using arguments of symmetry and energy minimization. Our results open the possibility to study novel topological defects in unusual environments, which do not have to be intrinsically superconducting or exposed to magnetic fields.

The authors thank Vetle Kjær Risinggård for useful discussions. This work was partly supported by the Research Council of Norway through its Centres of Excellence funding scheme, Project No. 262633, “QuSpin.” J.L. and J.A.O. also acknowledge funding from the Research Council of Norway Grant No. 240806.

\* morten.amundsen@ntnu.no

[1] A. A. Abrikosov, *J. Phys. Chem. Solids* **2**, 199 (1957).  
 [2] G. Blatter, M. V. Feigel'man, V. B. Geshkenbein, A. I. Larkin, and V. M. Vinokur, *Rev. Mod. Phys.* **66**, 1125 (1994).  
 [3] H. Suderow, I. Guillamon, J. G. Rodrigo, and S. Vieira, *Supercond. Sci. Technol.* **27**, 063001 (2014).  
 [4] D. Roditchev, C. Brun, L. Serrier-Garcia, J. C. Cuevas, V. H. L. Bessa, M. V. Milošević, F. Debontridder, V. Stolyarov, and T. Cren, *Nat. Phys.* **11**, 332 (2015).

[5] J. C. Cuevas and F. S. Bergeret, *Phys. Rev. Lett.* **99**, 217002 (2007).  
 [6] K. Usadel, *Phys. Rev. Lett.* **25**, 507 (1970).  
 [7] A. Di Bernardo *et al.*, *Phys. Rev. X* **5**, 041021 (2015).  
 [8] S. Mironov, A. Mel'nikov, and A. Buzdin, *Phys. Rev. Lett.* **109**, 237002 (2012).  
 [9] H. J. Fink and A. G. Presson, *Phys. Rev.* **151**, 219 (1966).  
 [10] L. F. Chibotaru, A. Ceulemans, V. Bruyndoncx, and V. V. Moshchalkov, *Nature (London)* **408**, 833 (2000).  
 [11] L. F. Chibotaru, A. Ceulemans, V. Bruyndoncx, and V. V. Moshchalkov, *Phys. Rev. Lett.* **86**, 1323 (2001).  
 [12] L. F. Chibotaru, A. Ceulemans, G. Teniers, and V. V. Moshchalkov, *Physica (Amsterdam)* **369C**, 149 (2002).  
 [13] J. Rammer and H. Smith, *Rev. Mod. Phys.* **58**, 323 (1986).  
 [14] W. Belzig, F. K. Wilhelm, C. Bruder, G. Schön, and A. D. Zaikin, *Superlattices Microstruct.* **25**, 1251 (1999).  
 [15] M. Y. Kupriyanov and V. F. Lukichev, *Zh. Eksp. Teor. Fiz.* **94**, 139 (1988) [*Sov. Phys. JETP* **67**, 1163 (1988)].  
 [16] N. Schopohl, [arXiv:cond-mat/9804064](https://arxiv.org/abs/cond-mat/9804064).  
 [17] M. Amundsen and J. Linder, *Sci. Rep.* **6**, 22765 (2016).  
 [18] See the Supplemental Material at <http://link.aps.org/supplemental/10.1103/PhysRevLett.120.207001> for a calculation of the giant vortex energies, an analytical solution of the Usadel equation in a current-carrying superconductor, and numerical results for asymmetric geometries. The Supplemental Material includes Refs. [19–22].  
 [19] K. Fossheim and A. Sudbø, *Superconductivity: Physics and Applications* (John Wiley & Sons, Chichester, 2004), Sec. 4.7.  
 [20] J. P. Morten, Master's thesis, Norwegian University of Science and Technology, Trondheim, Norway, 2003.  
 [21] S. H. Jacobsen, J. A. Ouassou, and J. Linder, *Phys. Rev. B* **92**, 024510 (2015).  
 [22] W. Hu, K. Sarveswaran, M. Lieberman, and G. H. Bernstein, *J. Vac. Sci. Technol. B* **22**, 1711 (2004).  
 [23] S. V. Bakurskiy, N. V. Klenov, I. I. Soloviev, M. Y. Kupriyanov, and A. A. Golubov, *Phys. Rev. B* **88**, 144519 (2013).  
 [24] J. Romijn, T. M. Klapwijk, M. J. Renne, and J. E. Mooij, *Phys. Rev. B* **26**, 3648 (1982).  
 [25] I. V. Grigorieva, W. Escoffier, V. R. Misko, B. J. Baelus, F. M. Peeters, L. Y. Vinnikov, and S. V. Dubonos, *Phys. Rev. Lett.* **99**, 147003 (2007).  
 [26] G. Teniers, L. F. Chibotaru, A. Ceulemans, and V. V. Moshchalkov, *Europhys. Lett.* **63**, 296 (2003).  
 [27] P. G. de Gennes, *Superconductivity of Metals and Alloys* (W.A. Benjamin, New York, 1966).  
 [28] F. S. Bergeret and J. C. Cuevas, *J. Low Temp. Phys.* **153**, 304 (2008).